Integrated geophysical investigation for mapping of manganese-iron deposits at Wadi Al Sahu area, Sinai, Egypt—a case study

Sultan Awad Sultan Araffa[1] · Taha Tawfik Taha Rabeh[1] · Salah El-Deen Abdel Wahab Mousa[2] ·
Sami Hamed Abdel Nabi[2] · Mohamed Al Deep[1]

Abstract

This study used data from an investigation into the mapping of manganese-iron (Mn-Fe) mineralization, located within the Um Bogma formation. The ore takes the form of patchy isolated bodies or lenses in the three members of the Um Bogma formation located in East Sinai, Egypt. Magnetic, resistivity, and induced polarization (IP) surveys were applied at the Wadi Al Sahu area to delineate the mineralized ore bodies in terms of depth and extension. The quantitative interpretation of magnetic data was carried out using the 2D analytical signal. The results of the magnetic interpretation indicated that the depths of such ore deposits range from -2 to -20 m, and the shape of the magnetized units (assumed to be manganese-iron ore) is lenticular and of small size ranging from 20 to 100 m in width. Three dipole-dipole geo-electrical traverses were carried out along the anomalous sites, the traverse locations selected from the constructed magnetic maps of the study area, and the resistivity and IP measurements along with them. The results of the resistivity and IP inversion indicate that there are conductive and chargeable bodies at a depth that indicate the shape of small Mn-Fe lenses being present and conform to the shape of the Mn-Fe ore mineralization. Integration between the magnetic and geo-electrical data is made to lessen the non-uniqueness problem in geophysical prospecting. In this case, we used electrical resistivity and induced polarization models to delineate the boundaries between different geo-electric units, and these boundaries were used as interfaces between layers with different magnetic susceptibility for magnetic modeling to perform magnetic data inversions.

Keywords Mineral exploration · Analytic signal · Electric methods · Magnetics methods · Mn-Fe minerals

Introduction

The study area is bounded by latitudes 28° 58′ 13″ and 28° 59′ 5″ N and longitude 33° 22′ 15″ and 33° 23′ 4.5″ E. The area is in the western Sinai near the town of Abu Zenima, Egypt (Fig. 1a). In the past, the manganese-iron ore stratigraphy was studied by Mart and Sass (1972), Kora (1984), and El Sharkawi et al. (1990), and geochemically studied by Ibrahim and Seif (2014) and many authors debated the origin of the ore, such as Gindy (1961), Nakhla and Shehata (1963), and Saad et al.

(1991). The mineralogical study was carried out by El Shazly and Saleeb (1959).

In this study, three geophysical techniques, including magnetic, induced polarization (IP), and resistivity were applied as these are important techniques in mineral exploration as well as many integrated geophysical methods used for mineral exploration (Smith 2002). The IP technique is used for mineral exploration, as well as for hydrological and environmental geological studies, e.g., Vacquier et al. (1957), Marshall and Madden (1959), Sumner 1976, Klein and Sill (1982), Towel et al. (1985), and Sternberg and Oehler (1990). Besides, Ramadan and Sultan (2004) used the magnetic technique, for identifying massive sulfide zones.

A combination between magnetic and electric methods was implemented by Mousa et al. (2020) to detect the distribution of titanomagnetite ore in southeastern Egypt; they summarized that metallic ores are ideal cases to study the similarity between geophysical methods.

✉ Mohamed Al Deep
    mohamed-abdelsabour@outlook.com

1   National Research Institute of Astronomy and Geophysics, Helwan, Cairo, Egypt

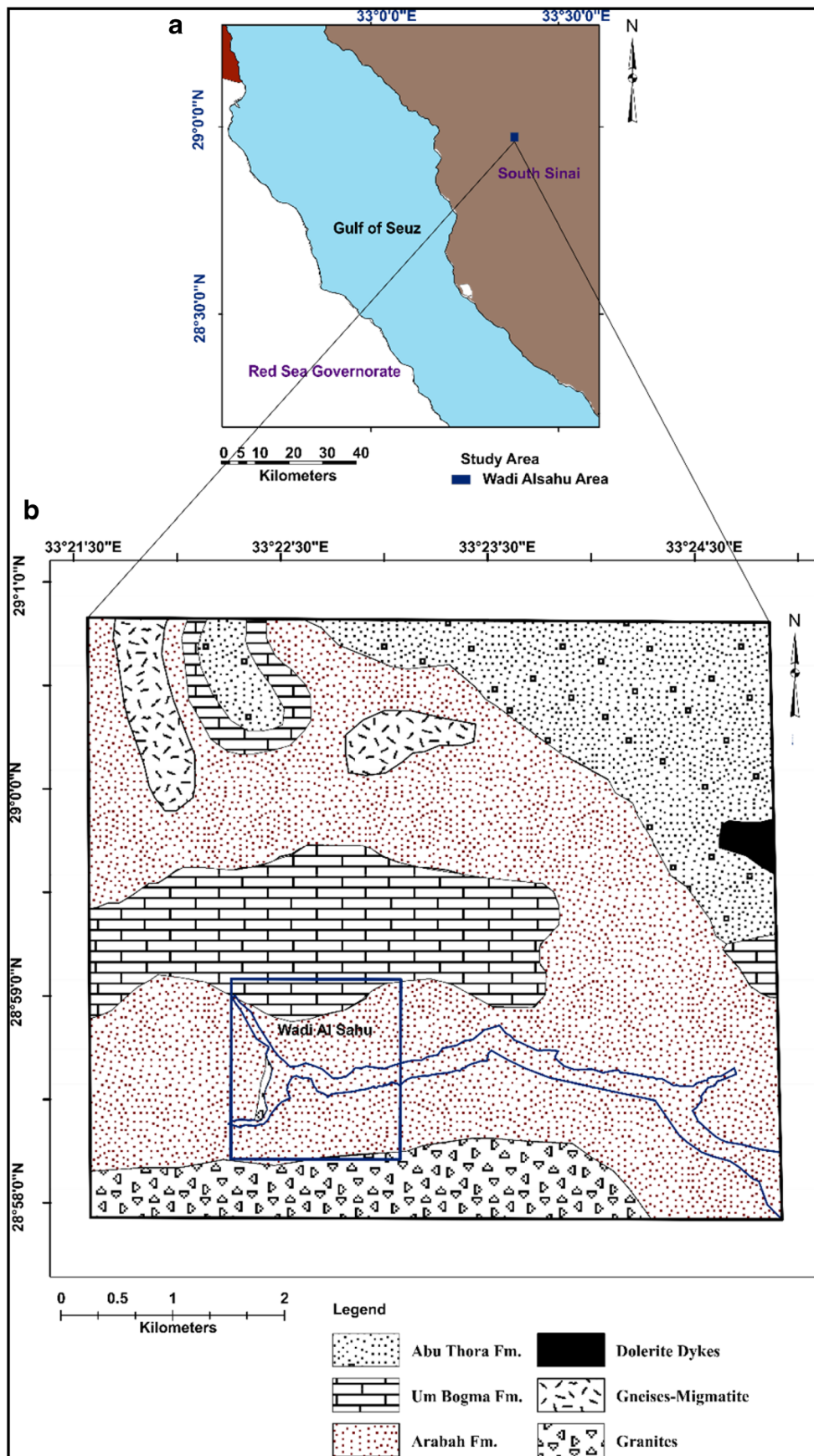2   Faculty of Science, Ain Shams University, Cairo, Egypt

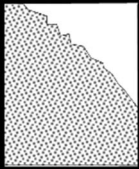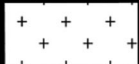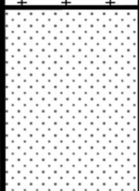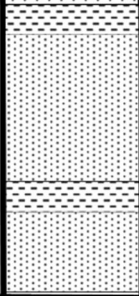**Fig. 1** **a** Location map. **b** Geological map of the studied area
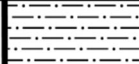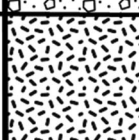
Age	Formation	Lithology		Environment
Permo-Triassic	Budra or Qiseib (0-160 m.)		Red beds; pebbly sandstones and mudstones in finiting upward cycles	Fluviatile
	Basalt (0-40 m.)		Basaltic sill intrusion and lava flows.	
Carboniferous	Abu Thora (30-200)		Glass sand member "Cross bedded" Kaolinitic claystone member "plant remains, coal and rare brachiopods"	Fluviatile, swampy to coastal marine
	Um Bogma (0-41 m.)		Sandy dolostone Marly dolostone (brachiopods, corals, etc.) Pink dolostone Mn-Fe ore	Shallow open marine
Cambro-Ordovician	Adedia (0-40)		Cross-bedded sandstone	Fluviatile
	Nasib (12-18 m.)		Thin-bedded silty sandstone (trace fossils).	Intertidal- deltac
	Abu Hamata (12-18 m.)		Shale and siltstone with Cruziana.	Shallow marine
	Sarabit ElKhadim (12-23 m.)		Pebbly arkosic sandstone	Intertidal Fluviatile
Precambrian Basement			Ignious and metamorphic rocks	

Fig. 2 Lithologic column of studied area

All the above authors used geophysical tools for mineral exploration, and some of such geophysical techniques are used for the detection of manganese-iron ore deposits located in the Wadi Al Sahu area, Sinai, Egypt.

Geological settings, and mineralogy

The study area is covered by a sedimentary sequence formed during the early Carboniferous and was later affected by the
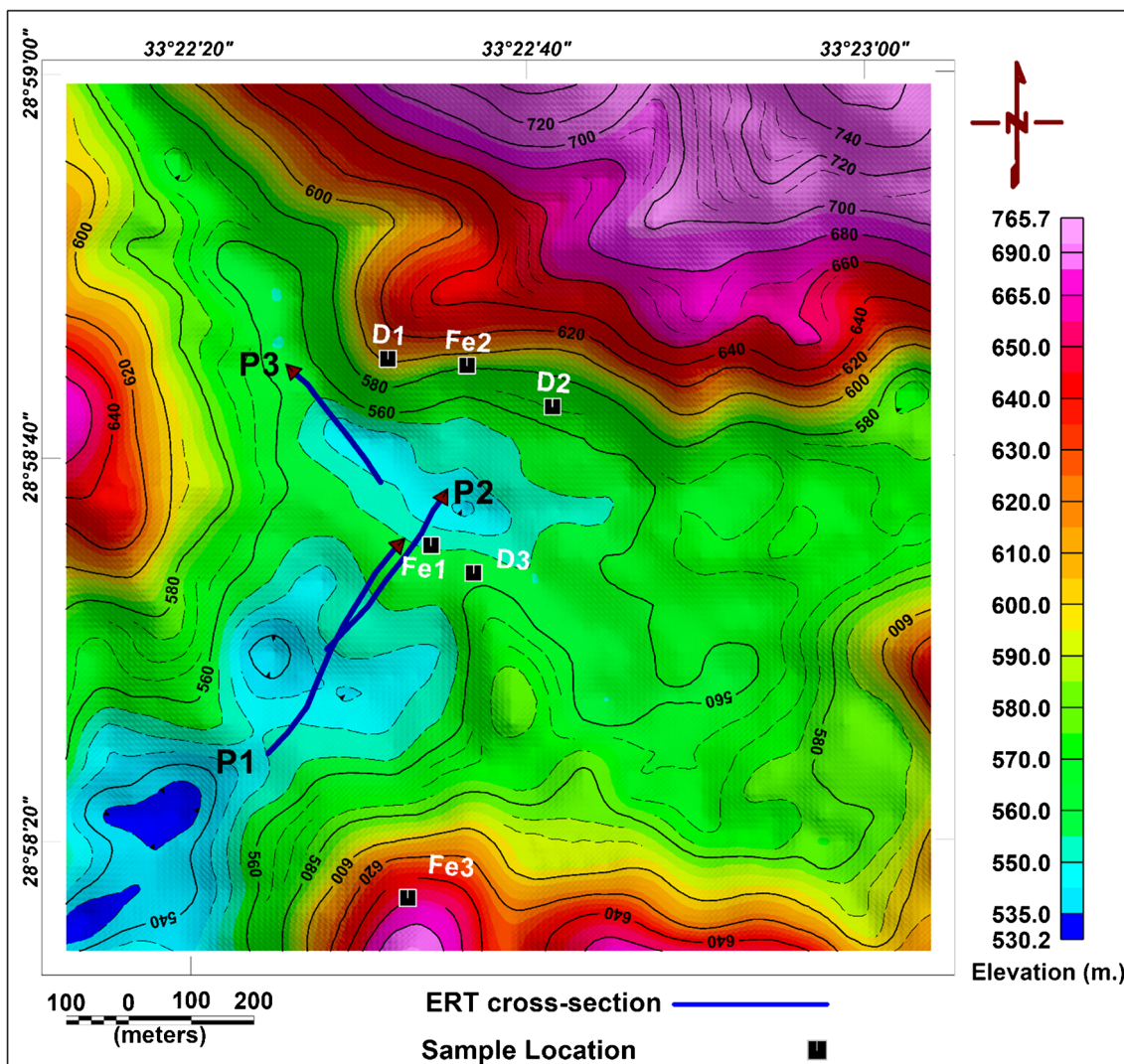
Fig. 3 Topography of Wadi Al Sahu with electric cross-section plot and the location of samples collected for petrophysical study

Oligo-Miocene basalt extrusion as shown in the geological map (Fig. 1b) according to El Shazly and Saleeb (1959). The Mn-Fe ore lenses occur within the three members of the Um Bogma formation which comprises dolomitic limestone (Fig. 2). The ore bodies vary in composition from pure manganese ore to pure iron ore; pyrolusite and manganite are the most widely distributed and predominant among the manganese minerals, but psilomelane and cryptomelane are less common, the iron minerals are more abundant in Sinai, and they are essentially represented by goethite and less hematite, but usually, it is a mixture of the two ores in varying concentrations. Especially in the larger lenses, i.e., those with diameters larger than 50 m, a division into three geochemical zones is recognized as stated by Mart and Sass (1972). These

Table 1 Magnetic susceptibility for the samples collected from Wadi al Sahu area

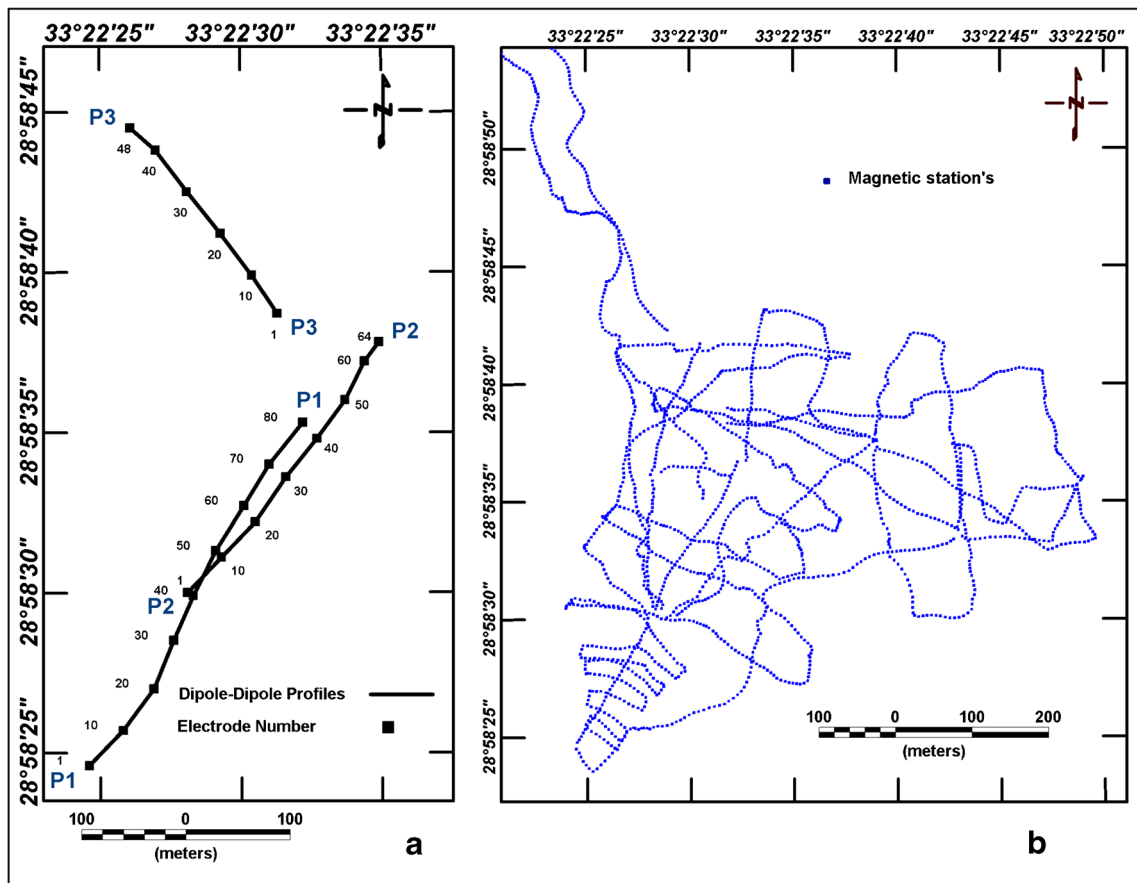| Sample type	Location (degrees)		Sample	Susceptibility (CGS units)	
	Latitude	Longitude			
Mn-Fe ore	28.9764996	33.3762016	Fe1	0.002625	The average 0.00539 CGS
	28.9790993	33.3768005	Fe2	0.007702	
	28.9713993	33.3758011	Fe3	0.005869	
Dolomitic limestone	28.9792004	33.3754997	D1	0.000083	The average 0.000090 CGS
	28.9785004	33.3782005	D2	0.000079	
	28.9761009	33.3768997	D3	0.000109	

Fig. 4 **a** Location map of the geo-electric survey in the studied area. **b** Detailed geomagnetic survey in the studied area
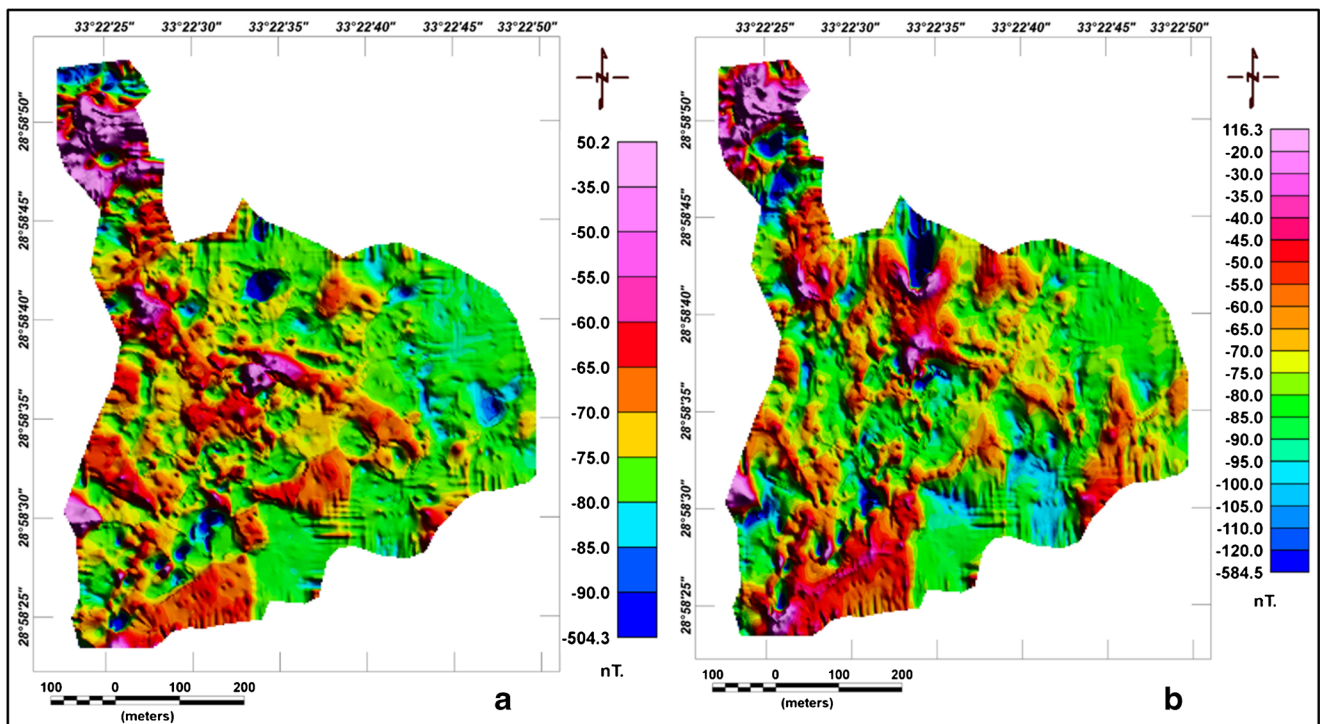

Fig. 5 **a** The total magnetic field map after applying diurnal correction. **b** The reduced to pole magnetic map
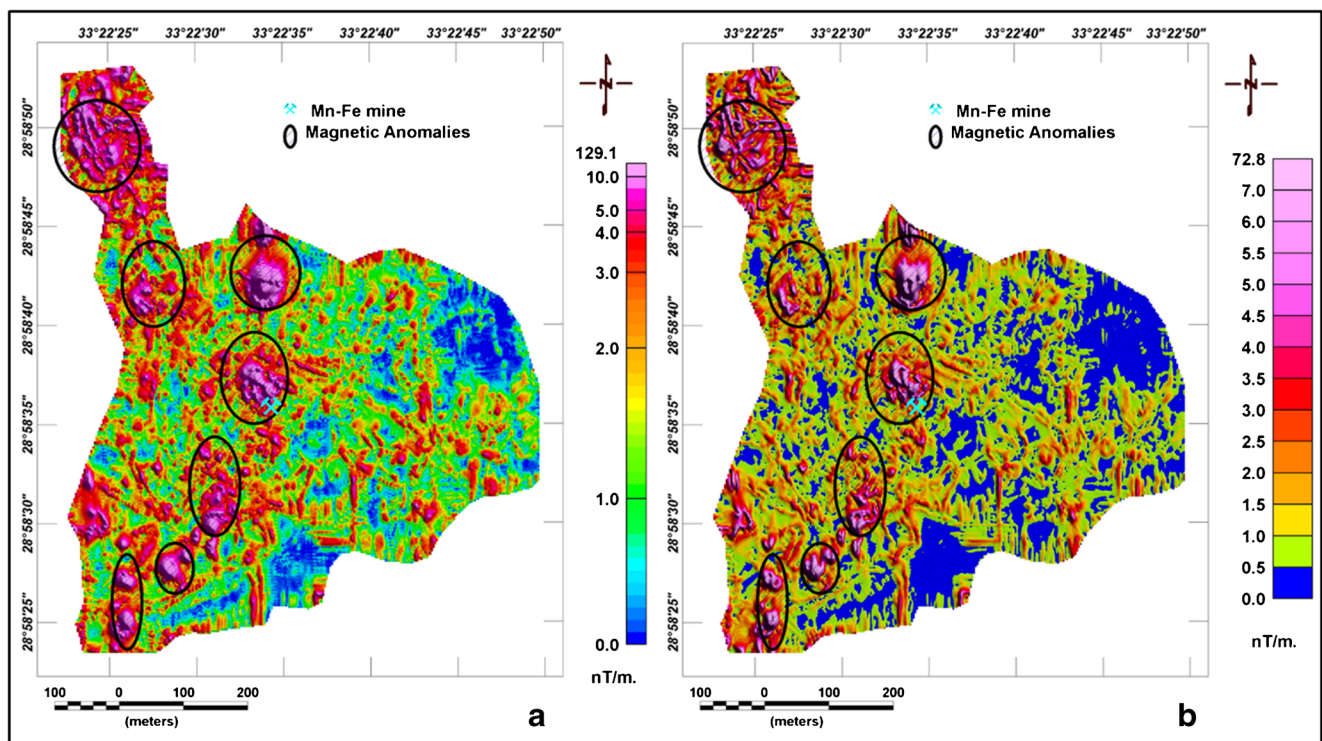
Fig. 6 **a** The analytic signal map. **b** The total horizontal gradient map. Both maps showing the exact location of anomalies with a present mining location and circles to show areas with the same magnetic signature

rock units include (1) an inner manganiferous zone, (2) an intermediate ferruginous-manganese zone, and (3) an outer ferruginous zone. The general topography is shown in Fig. 3, representing Wadi Al Sahu surrounded by hills ranging in elevation between 500 and 850 m.

The origin of the studied manganese deposits in Um Bogma area resembles the same ore in most of Africa; there are three theories that are defined (Gindy 1961, Nakhla and Shehata 1963, Saad et al. 1991), maintaining the view that the manganese ores are of epigenetic origin, which is a result of the activity of ascending mineralized hydrothermal solutions through the host rock, and on the other hand (Mart and Sass 1972; Magaritz and Brenner 1979; Kora 1984), have advocated a primary sedimentary-type of manganese ore; this type of deposit is identified in other regions such as in Africa, for example, the Kalahari deposit, namely low-grade primary sedimentary Mamatwan-type ore, containing between 20 and 38 wt% manganese metal, and secondary high-grade Wessels-type ore containing 45–60 wt% manganese metal as mentioned in the manganese adventure by Cairncross et al. (1997). The third theory stated by E1 Sharkawi et al. (1990) demonstrated the role of weathering in the accumulation of the manganese deposits during the mature stage of Carboniferous karstification, highly oxidized ore minerals.

Many samples of manganese-iron ore and the surrounding rocks were collected from the excavated site in the study area, on which the magnetic susceptibility was measured by MS2B susceptibility meter. The location and measured susceptibility in units of each sample are given in Table 1; the measurements are found to be ranging between 0.00009 for dolomitic rocks and 0.0053 for the manganese-iron ore in CGS units.

Geophysical surveys

The Mn-Fe ore occurs in a wide area in western Sinai, but only a certain area was selected for the present magnetic and geo-electrical surveying. These geophysical techniques will be used to gain a better understanding of the correlation between Mn and Fe and the nature of the ore. The detailed geophysical survey is shown in Fig. 4 a and b.

The total field magnetic survey was achieved by using an Overhauser magnetometer model (GSM-19FG) with a built-in navigation system (2012). A total of 6348 measured magnetic stations were accomplished. The magnetic measurements were collected in the continuous mode along the traverses with 2-m station separation. The base station recordings were carried out using a proton precision magnetometer.

Three electrical resistivity tomography (ERT) profiles and induced polarization (IP) cross-sections were made within the study area; two of them trend northeast-southwest and the third is oriented perpendicular to this direction (Fig. 4). Measurements carried out by using the dipole-dipole array of electrode spacing of 5, 10, and 15 m using an IRIS

resistivity and IP system (the Syscal R2). The ERT method is used to identify the ore bodies from the surrounding rocks by resistivity contrast, whereas the IP method is used to differentiate between massive and disseminated ore bodies utilizing the chargeability variation.

Processing and interpretation

The magnetic response is indicative of rock types with different magnetic susceptibilities, and by differentiating between highly and lowly magnetized geology, it is possible to find the contacts between different magnetic rock types. The magnetic data was corrected by removing the diurnal variation as well as correcting for the secular variation, by which the IGRF model has been removed. Figure 5 a shows the magnitude of magnetic anomalies in the total magnetic field map after the correction stated before which varies from ($-$ 504.3 to 50.2 nT). Figure 5 b shows the magnitude of magnetic anomalies in the reduced to the pole map (RTP) which varies from $-$ 584 to 117 nT; however, they are much smaller over the individual magnetic bodies, and the anomalies are distributed mostly in the western and middle part of the surveyed area. The maximum amplitudes of anomalies are concentrated in the southern, middle, and northern parts of the study area. The IGRF field parameters used to calculate the RTP map are ($H =$ 43,226.7 nT, $I = 43.1°$, $D = 4.1°$).

The analytic signal map (Fig. 6a) is obtained from the total field magnetic data. The analytic signal is a useful tool used for locating magnetic sources because of the bipolar nature of the magnetic field. The analytic signal filter was applied to the magnetic data using Eq. (1) of Roest et al. (1992):

$$A(x, y, z) = \sqrt{\left(\frac{\delta H}{\delta x}\right)^2 + \left(\frac{\delta H}{\delta y}\right)^2 + \left(\frac{\delta H}{\delta z}\right)^2} \qquad (1)$$

The amplitude of the horizontal gradient Cordell and Grauch (1985) is expressed as Eq. (2).

$$\text{Horozontal gradient} = \sqrt{\left(\frac{\delta H}{\delta x}\right)^2 + \left(\frac{\delta H}{\delta y}\right)^2} \qquad (2)$$

where H is the total magnetic field, and $\left(\frac{\delta H}{\delta x}\right)$, $\left(\frac{\delta H}{\delta y}\right)$, and $\left(\frac{\delta H}{\delta z}\right)$ are the directional derivatives of the magnetic field at x, y, and z respectively.

The analytic signal is similar to the total horizontal gradient (THG) in the shape and distribution of anomalies. The magnitude of the analytical signal map ranges from zero to 129.1 nT/m. The magnitude of the THG map (Fig. 6b) ranges from zero to 72.8 nT/m. The higher magnitudes are found within the central part of the survey area, also to the northeast and the
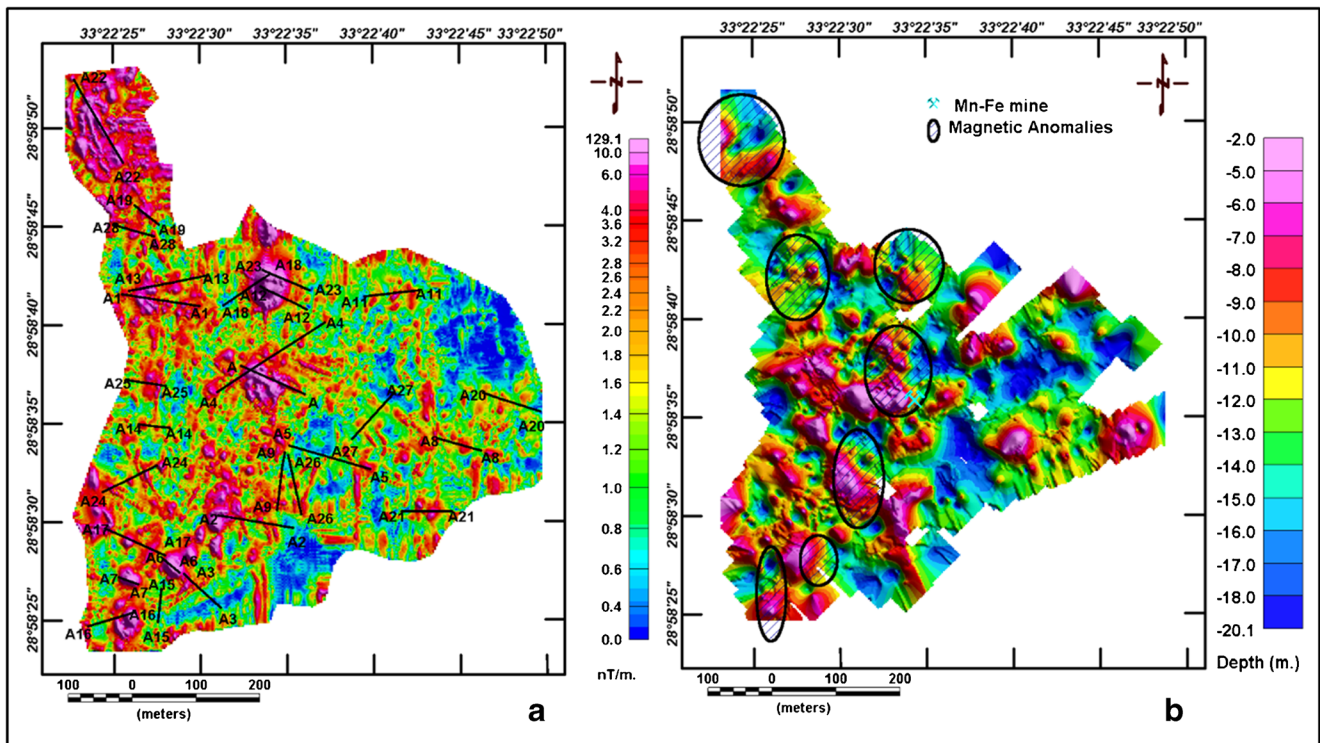

Fig. 7 a Selected profiles along major anomalies in the studied area with the analytic signal map as a background. b The calculated depth map by 2D analytic signal
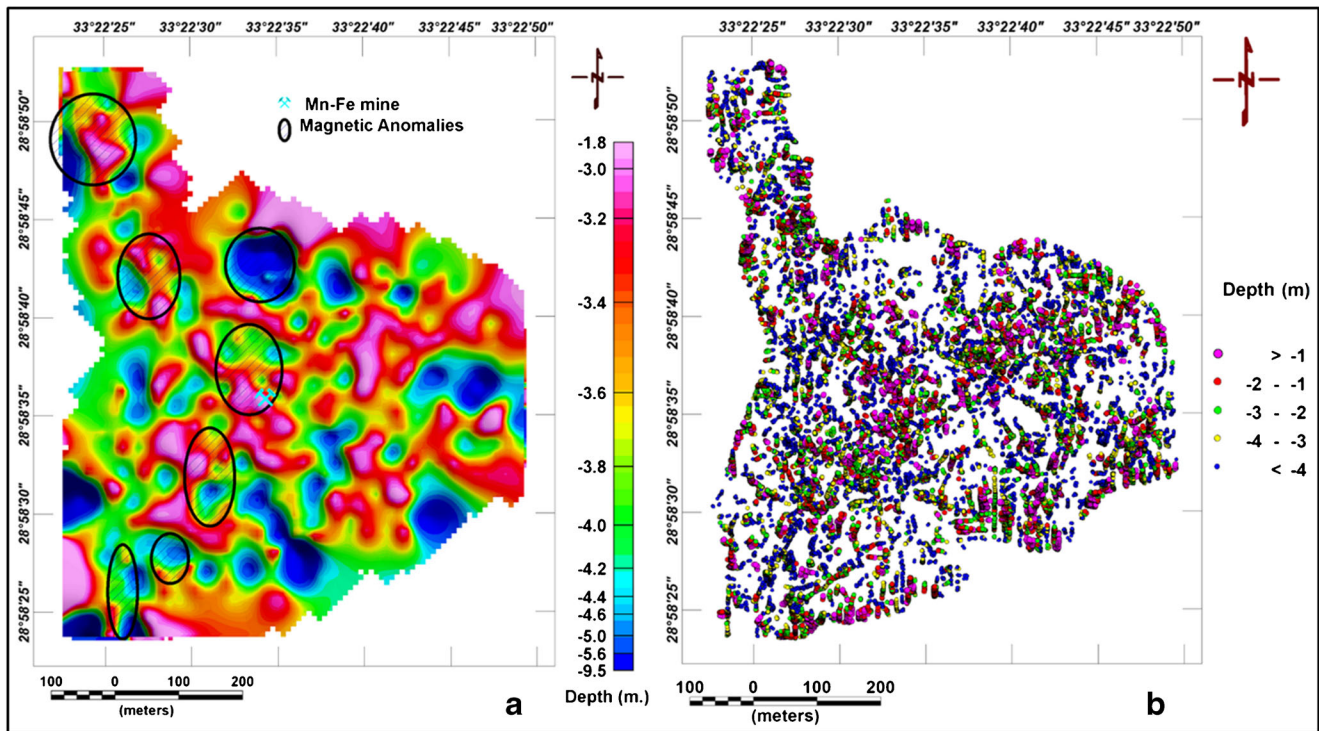
Fig. 8 a Depth to magnetic source calculated by source parameter imaging technique. b Symbol plot of the calculated Euler solutions with (SI = 1)

southwest, with two more anomalies to the west. Small anomalies are dispersed around the area but not of economic importance. Presently, mining is coinciding with one of the high amplitude bodies, and as such, we used similar magnetic signatures to delineate areas for further investigation. From the petrophysical analysis of the ore and the surrounding rocks, we can conclude that the higher magnetic susceptibility of iron-manganese ore relative to dolomitic limestone can produce a relatively small amplitude magnetic anomalies; also, we expect these anomalies to have the shape and size reflecting the ore occurrence; from the interpretation of the analytic signal and the THG map, we can detect some anomalies that can be related to Mn-Fe ore lenses as expected.

The analytical signal depth analysis was used to calculate the depth to the magnetic (or gravity) sources; this method was first applied by Phillips (1997), even though the theoretical aspect of this method is suggested by Nabighian (1972, 1974).

Many authors have derived a generalization formulation for depth estimation from the analytic signal, Shu-Kun et al. (1998) and Ibrahim (2008), for example; the magnetic anomaly T(x) at any observation point P(x) along a profile crossing a magnetized step-like body can be described by the following equation derived from Nabighian (1972)

$$T(x) = \alpha[(\theta_1 - \theta_2)\cos\varphi + \sin\varphi ln(r_1/r_2)] \tag{3}$$

where $\alpha = 2kHc \sin d$, k is the susceptibility contrast, H the geomagnetic field intensity, (d) is the dip angle of the corner

of the step, (t) is the thickness of the step, and (h) is the depth to the top of the step. By differentiating Eq. (3) concerning x and taking t to infinity leads to Eq. (4). Similarly, differentiating Eq. (3) concerning z and taking t to infinity, we can obtain the vertical derivative in Eq. (5):

$$T_x(x) = \frac{\partial(T)}{\partial x} = \alpha \frac{(h-z)\cos\varphi + x\sin\varphi}{(h-z)^2 + x^2} \tag{4}$$

$$T_z(x) = \frac{\partial(T)}{\partial x} = \alpha \frac{x\cos\varphi + (h-z)\sin\varphi}{(h-z)^2 + x^2} \tag{5}$$

$T_x(x)$ and $T_z(x)$ is the Hilbert transform for the magnetic field with respect to x and z, respectively; the analytic signal can be obtained from Eqs. (4), and (5) as follows:

$$A(x) = T_z(x) - iT_x(x) \tag{6}$$

Simplifying Eq. (6), we obtain

$$A(x) = \frac{\alpha\, e^{i\varphi}}{h + ix} \tag{7}$$

Equation (7) links the analytic signal directly to the depth to the top of magnetized bodies (h).

To calculate the depth solutions from the analytic signal, we use Geosoft Oasis montaj (2015), The calculations were made using two methods, first by selecting profiles along with the major anomalies from the gridded dataset and calculated the depth from the AS (Fig. 7a, b) where the calculated depths were found to be ranging between 2 and 20 m. The symbol
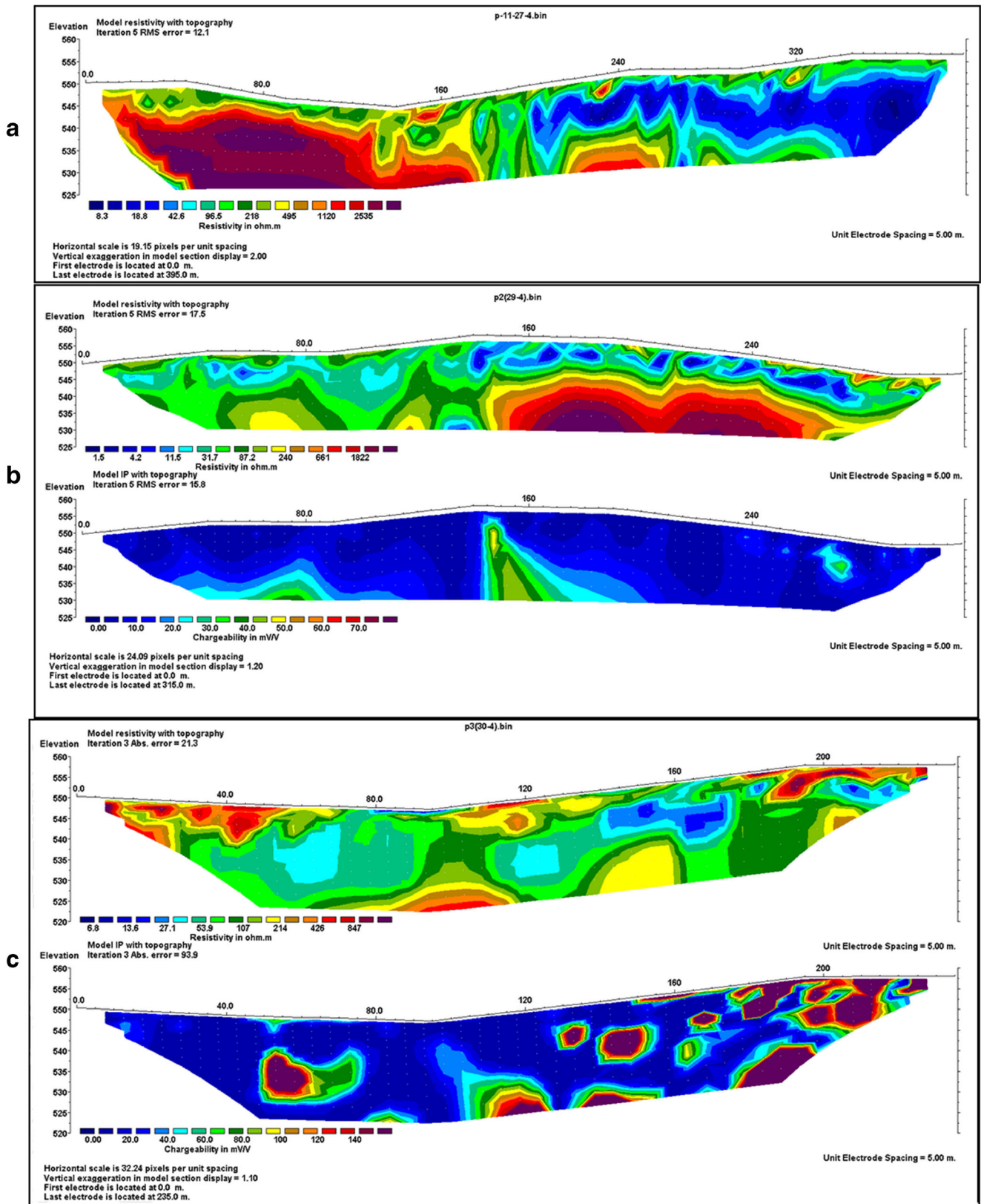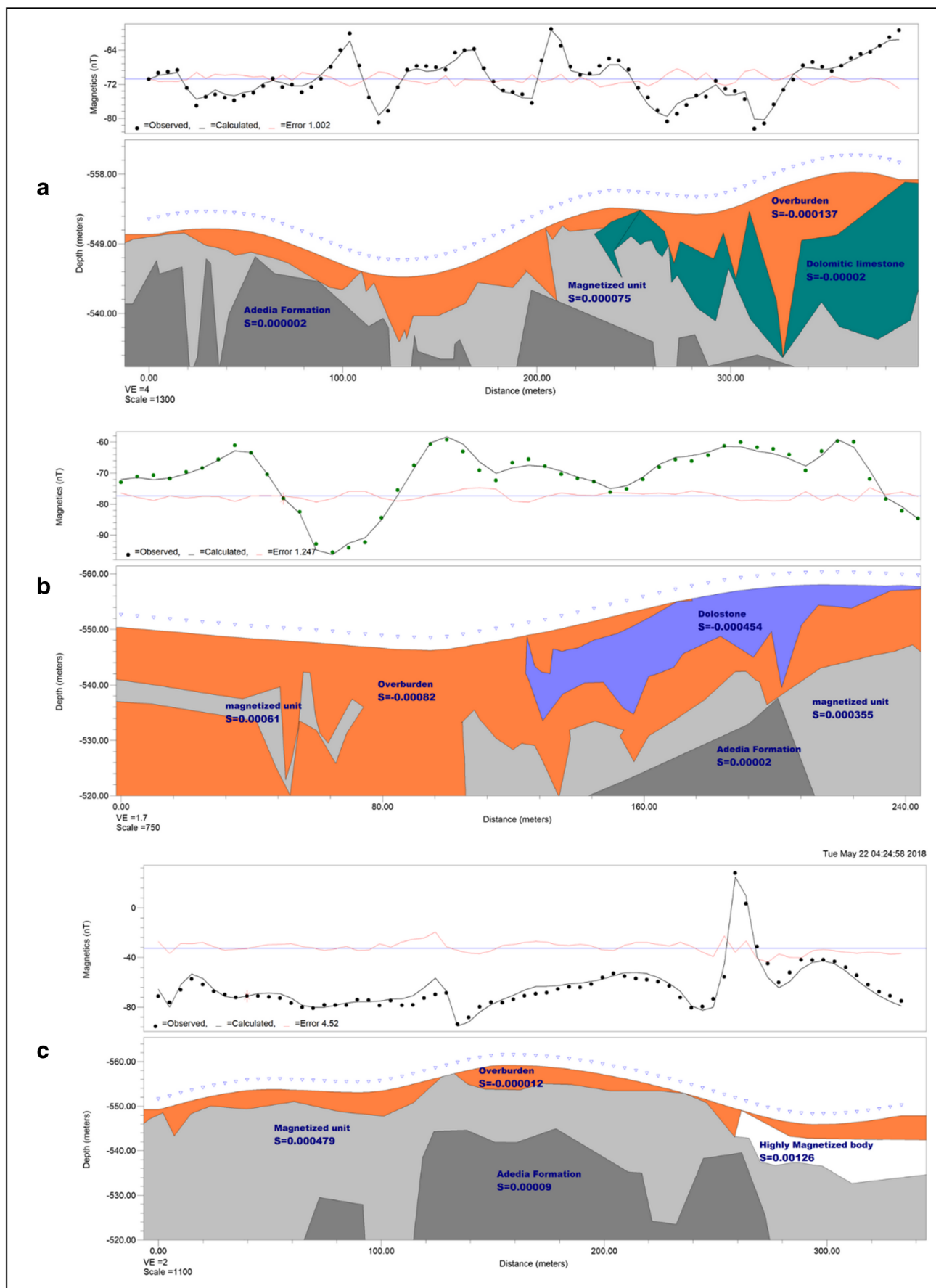
Fig. 9 **a** The resistivity model for cross-section no. 1. **b** The resistivity and IP model for cross-section no. 2. **c** The resistivity and IP model for cross-section no. 3

◀ **Fig. 10** **a** Model of magnetic profile no.1 traced over the ERT cross-section no.1. **b** Model of magnetic profile no. 2 traced over the ERT cross-section no. 2. **c** Model of magnetic profile no. 3 traced over the ERT cross-section no. 3

shows where present mining areas are located on the map, indicated by circles and ellipses with a fixed location drawn to show the suggested sites for further excavation and extraction.

The source parameter imaging technique was developed for automated depth calculation; it is used on gridded magnetic data. This method characterized by the calculated depth results is not affected by the magnetic inclination and declination, so it is not necessary to use a pole-reduced input grid.

The SPI method developed after Thurston and Smith (1997) was use as a step-type source model to calculate depth to magnetic sources in a gridded dataset; in this case, the following formulas are applied:

$$k = \sqrt{\left(\left[\frac{dA}{dx} \right]^2 + \left[\frac{dA}{dy} \right]^2 \right)} \qquad (8)$$

where k is the local wavenumber over the step-type source, and A is the tilt derivative and the depth can be calculated using the given simple equation

$$depth = \frac{1}{k\ max} \qquad (9)$$

where $k\ max$ is the maximum peak value of k over the step-type estimated source. The calculated depth map was showed in Fig. 8 a and we can notice that the depth values estimated by this technique range from 1.8 to 10 m from the ground surface. The depth values are similar for the different methods. There are three main groups of magnetized bodies located in the central part, northwestern, and in the southwestern part; the detected body can be represented as an arch from some circles which center to the west; the pattern can be related to structural origin or the sedimentary environment during deposition. The depth patterns are resembling those calculated by Euler

Fig. 11 Integrated interpretation map for the geological and geophysical results
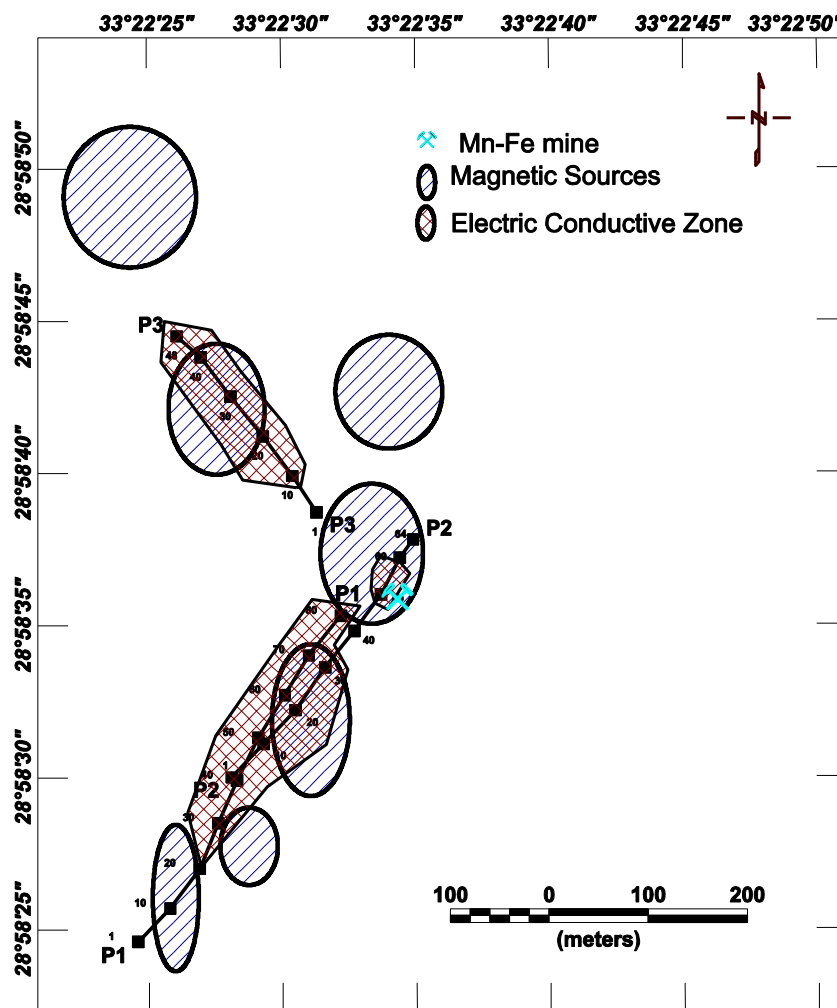
deconvolution with the structural index (SI) equal to one, where the lower depth symbol clusters are located above areas with minimum depth on the SPI depth map and shown in Fig. 8b.

From the inspection of the results obtained from SPI and 2D analytic signal, we can notice that both methods give similar results, which can explain as follows: both methods do not distress by inclination and declination of the induced magnetic anomaly.

The processing and interpretation of the obtained data were carried out using the RES2DINV (2003) program, which produced an image of the electrical resistivity distribution in the subsurface based on a regularization algorithm (Loke and Barker 1996) that produced an interpretive image down to a depth of 25 m.

The dipole-dipole cross-section of length 395 m along with magnetic profile no. 1 as shown in Fig. 9 a measured resistivity without IP and reach a maximum depth of about 25 m. From a visual inspection, the resistivity distribution on the southwestern part consists of a very resistive part which may indicate dry cross-bedded sandstone of Adedia Formation with a high resistivity overlain by moderately resistive overburden. On the northeastern part of the section resides a sheet-like low resistivity body and thought likely to be a manganese-iron ore body which occurs mainly as lenses in the three members of the Um Bogma formation. The postulated lens length is about 180 m and its thickness varies from point to point reaching its greatest thickness of about 15 m towards the northeastern end of the section. The dipole-dipole cross-section along profile no. 2 (Fig. 9b) depicts the measurements for resistivity and IP; the total length of the section is about 315 m. The section covers a maximum depth of about 25 m.

From a visual inspection, the resistivity section shows a resistivity high at depth in the northeastern part overlain by a conductive layer of about 7 m thick which could indicate also a thin wedge or Mn-Fe mineralization. The southwestern part of the section depicts a completely different resistivity pattern and the two distinct patterns may be separated by a fault plane dipping to the northeast. The IP section has mostly a very small chargeability except over the suspected contact zone where it becomes moderate between the two geological sequences and this feature could also indicate the presence of a fault. A moderate chargeability is also observed over the thickest part of the suspected mineralization to be present on the northeastern side. These other disseminated bodies are of 20 m width at a shallower depth below the ground surface. Furthermore, three small units located at distance 245–285 m from the beginning of the cross-section distributed horizontally parallel to the earth surface are likely to be small lenses characterized by low resistivity and relatively moderate chargeability values. The dipole-dipole cross-section along profile no. 3 (Fig. 9c) is 235 m of total length and reaches its largest depth of about 30 m from the visual inspection of the

resistivity, and IP value distribution of this section indicates a resistivity pattern more similar to that of the southwestern part of profile no. 2 which is a patchy low to a high resistivity body with relatively high chargeability, and when taking into account the previous cross-sections, it is likely to be a disseminated manganese-iron ore body. Most of the bodies as shown in the section have dimensions of about 20 m in width. The suspected disseminated ore zones begin at 40 m from the line start and continue up to the end of the profile. The highest resistivity values are related to the host rock, which is a massive granitic rock unit. This conclusion can be ensured with the IP model from chargeability, which indicates a patchy ore body and several disseminated small lenses.

The most conflicting problem in geophysical interpretation is the non-uniqueness problem, which occurs when more than one Earth model can explain the same set of geophysical data. To overcome such a problem, three inverted magnetic profiles were abstracted over the three geo-electrical cross-sections in the same location and with the same length (see Fig. 2). The GM-SYS inversion routine utilizes a Marquardt inverse modeling algorithm (Marquardt 1963) to linearize and invert the calculations; the resulting model is a simple magnetic susceptibility model that can be related to subsurface geology. GM-SYS uses an implementation of that algorithm for gravity and magnetic modeling developed by the USGS. In a model in Fig. 10a, the resistivity models from the geo-electrical profile no. 1 are used as background images in the model window through the precise location relative to x, y, and z. The product of inversion should not be exact as the resistivity model, so the inversion led to little change between the two models with very low root mean square value equal to 0.724%, which is an indicator of the misfit between the synthetic curve and the original magnetic data points in the magnetic inversion.

In model no. 2 shown in Fig. 10b, the inversion led to little change between the two models with very low root mean square value equal to 0.797%. In this profile, more attempts were needed to find the best-fitted model that can describe both resistivity and IP models. Model no. 3 shown in Fig. 10c has a little change between the two models with a low root mean square value equal to 0.671% in magnetic inversion. In this profile, more tries were needed to find the best-fitted model that can describe both resistivity and IP models, as well.

Results and discussion

Depth obtained with the 2D analytic signal method to the top of magnetic sources ranges from zero to a maximum of 20 m. The sources are of very small size with width range from 20 to 100 m. From the analysis of resistivity and IP models of the three cross-sections, we can determine four geological units that can be detected. The first unit is the uppermost weathered

and fractured zone which may or may not contain ore usually showing high resistivity and low chargeability. The second unit presents a massive ore body that characterized by a very low resistivity with elevated chargeability. The third unit is the sedimentary host rock which always gives moderate resistivity and no chargeability effect. Finally, the fourth unit is the basement rock with high resistivity and very low chargeability. The modeling of magnetic data using horizons from resistivity and IP models can be identical.

The result obtained from magnetic qualitative and quantitative analysis and the result of resistivity and IP inversion are summarized in a simple location map of the assumed manganese-iron ore bodies as shown in (Fig. 11); furthermore, we can refer to the magnetic susceptibility models generated by the GM-SYS program for the three cross-sections agreed with the resistivity and IP inverted models.

The aims of this research are as follows: (1) integration between geophysical exploration techniques for better detection of subsurface magnetized ores, and (2) detection of areas with very high probability as a potential source for the ore. The geologic setting of the ore bodies defines its occurrence as small lenses or patchy bodies dispersed in the three members of the Um Bogma formation (Fig. 3). The geophysical investigation detects sources of high magnetic susceptibility and high conductance in the same form. The results of magnetic data qualitative interpretation indicate multiple dispersed bodies within the study area concentrated within the center and to the southwest and northeast. Results of magnetic quantitative interpretation detected the top to magnetic sources ranging from 2 to 20 m. Results of geo-electric inversion indicated low resistivity and conductive bodies. Geophysical interpretation for exact and perfect results cannot be achieved depending on a single technique, and it will be more accurate and useful when integrated with other information to improve the interpretation process.

Conclusions

The results of the given study can be concluded as follows: (1) the study succeeded to detect mineralization zones with anomalies in the same shape described by geological studies for the ore outcrops and the area of Wadi Al Sahu has great potential in mineral content; we believe that there is a misunderstanding due to the structural origin of the valley that made all the exploration attempts during the past oriented to the ore outcrops, neglecting the subsurface ore deposits in the subsiding valleys. (2) The electric resistivity and induced polarization methods detect lenses of low resistivity and high chargeability that may be interpreted as ore bodies. (3) Results from the qualitative and quantitative interpretation of magnetic data detect the same shape of magnetic anomalies. (4) From the scientific point of view, the integration between geophysical methods can led to better calculation and more reliable results were achieved in this study. (5) Applying practical modeling for magnetic anomalies proves to be valuable by measuring the magnetic susceptibility of the ore and the surrounding rocks and use the measured values to differentiate between ore bodies and the surroundings in the modeling process.

References

Cairncross B, Beukes N, and Gutzmer J (1997) The manganese adventure. Associated Ore & Metal Corp Ltd. Johannesburg. pp236

Cordell L, and Grauch VJS (1985) Mapping basement magnetization zones from aeromagnetic data in the San Juan Basin, New Mexico, in Hinze, William J. (ed), The utility of regional gravity and magnetic anomaly maps: Society of Exploration Geophysicists, Tulsa, Oklahoma, (1985). pp. 181–197

El Sharkawi MA, El Aref MM and Abdel Motelib A (1990) Manganese deposits in a carboniferous paleokarst profile, Um Bogma region, west-central Sinai, Egypt: Mineral. Deposita, vol. 25, pp. 34–43

El Shazly EM, Saleeb GS (1959) Contributions to the mineralogy of Egyptian manganese deposits. Econ Geol 54(1959):873–888

Geosoft oasis montaje, V.8.2.4 (2015) Geosoft software for the earth sciences, Geosoft Inc., Toronto, Canada

Gindy AR (1961) On the radioactivity and origin of the manganese-iron deposits of west central Sinai. Egypt Acad Sci 16:71–86

Ibrahim Aydin (2008), Estimation of the location and depth parameters of 2D magnetic sources using analytical signals, J Geophys Eng, 5, 3, September 2008, Pages 281–289, https://doi.org/10.1088/1742-2132/5/3/004

Ibrahim HK, Seif RA (2014) Geochemistry of manganese- iron ores at um Bogma area, west central Sinai, Egypt. Int J Adv Sci Tech Res 6(4):258–283

Klein JD, Sill WR (1982) Electrical properties of artificial clay-bearing sandstone. Geophysics 47:1593

Kora M (1984) The Paleozoic outcrops of Um Bogma area, Sinai: Ph.D. thesis, Monsoura Univ., Egypt, p.280

Loke MH, Barker RD (1996) Rapid least-squares inversion of apparent resistivity pseudosections by a quasi-Newton method. Geophys Prospect 44:131–152

Marquardt DW (1963) An algorithm for least-squares estimation of nonlinear parameters. J Soc Ind Appl Math 11(2) (Jun.,1963):431–441

Marshall DJ, and Madden TR (1959) Induced polarization, a study of its causes. Geophysics 24:790–816

Mart J, Sass E (1972) Geology and origin of the manganese ore of Urn Bogma. Sinai Econ Geol 67:145–155

Magaritz M, Brenner IB (1979) The geochemistry of a lenticular manganese-ore deposit (Um Bogma, Southern Sinai). Mineral. Deposita 14:1–13. https://doi.org/10.1007/BF00201863

Mousa SAW, Abdel Nabi SH, Araffa SAS, et al. (2020) Geophysical exploration of titanomagnetite ore deposits by geomagnetic and geoelectric methods. SN Appl Sci 2, 444 (2020). https://doi.org/10.1007/s42452-020-2206-5

Nabighian MN (1972) The analytic signal of two-dimensional magnetic bodies with polygonal cross-section: its properties and use for automated anomaly interpretation. Geophysics 37(3):507–517

Nabighian MN (1974) Additional comments on the analytic signal of two-dimensional magnetic bodies with polygonal cross-section. Geophysics 39(1):85–92

Nakhla FM and Shehata MRN (1963) Mineralogy of some manganese-iron ores from west central Sinai, Egypt: N-Jb Miner., Abh. Vol. 99, N.3, pp. 277–294

Phillips JD (1997) Potential-field geophysical software for the PC, version 2.2: USGS Open- File Report, pp. 97–725

Ramadan TM and Sultan AS (2004) Integration of remote sensing, geological and geophysical data for the identification of massive sulphide zones at Wadi Allaqi area Middle East J., Ain

Roest WR, Verhoef J, Pilkington M (1992) Magnetic interpretation using the 3-D analytic signal. Geophysics 57:116–125

Saad NA, Zidan BI, Khalil IK (1991) Manganese ore deposits of west central Sinai, Egypt: its mineralogy and genesis. Alexandria University, Egypt, Second Geochemical Conference, pp 60–80

Shu-Kun Hsu, Dorothée Coppens, and Chuen-Tien Shyu (1998) Depth to magnetic source using the generalized analytic signal GEOPHYSICS, VOL. 63, NO.6 (NOVEMBER-DECEMBER 1998); P.1947–1957, 11 FIGS

Smith RJ (2002) Geophysics of iron oxide copper-gold deposits (hydrothermal iron oxide copper–gold and related deposits: a global perspective vol 2) ed T M Porter (Adelaide: PGC Publishing), pp. 357–67

Sternberg BK and Oehler DZ (1990) Induced polarization in hydrocarbon surveys: Arkoma basin case histories induced polarisation: applications and case histories vol 4, ed S H Ward (USA: Society of Exploration Geophysicists)

Sumner JS (1976) Principles of induced polarization for geophysical exploration (Amsterdam: Elsevier), p. 277

Thurston JB, and Smith RS (1997) Automatic conversion of magnetic data to depth, dip, and susceptibility contrast using the SPI(TM) method: Geophysics, 62, 807–813

Towel JN, Anderson RG, Pelton WH, Olhoeft GR and LaBrecque D (1985) Direct detection of hydrocarbon contaminants using induced polarization method SEG Meeting, pp. 145–7

Vacquier V, Holmes CR, Kintzinger PR and Lavergne M (1957) Prospecting for groundwater by induced electrical polarization Geophysics, 23, pp. 660–87